EasyChair Preprint

№ 12879

Co-Optimization for 3D Printing Graded-Density Porous Structure and Filling Path Based on Voronoi Skeletons

Lingwei Xia

April 3, 2024

Proceedings of the IASS 2024 Symposium
Redefining the Art of Structural Design
August 26-30, 2024, Zurich Switzerland
Philippe Block, Giulia Boller, Catherine DeWolf,
Jacqueline Pauli, Walter Kaufmann (eds.)

Co-optimization for 3D printing graded-density porous structure and filling path based on Voronoi skeletons

Lingwei XIA*

*College of Future Technologies
Hohai University, Nanjing 211100, China
Lingwei.xia@hhu.edu.cn

Abstract

Porous structures are widely utilized as functional components in multiple industries due to their excellent comprehensive properties. Compared with traditional production processes, 3D printing additive manufacturing exhibits a dominant advantage in flexibility and low expense for fabricating porous structures. However, the complicated geometric morphologies that are constituted by thin-walled elements decrease the mechanical performance of structures due to manufacturing issues. For this reason, a co-optimization method is proposed for designing and manufacturing graded-density porous structures. Manufacturing constraints related to the filling path are incorporated in the structural optimization. The material layout is optimized by graded-density Voronoi elements mapped by Young's modulus. Finally, the structure is filled by an evenly continuous path without any intersection based on Voronoi skeletons. This research provides a novel idea to enhance the stiffness and promote the integration of material-structure-performance for additive manufacturing porous structures.

Keywords: Material extrusion, Porous structure, Topology optimization, Path optimization, Manufacturing constraints.

1. Introduction

Porous structures are an important class of engineering solids, possessing superior comprehensive properties such as high stress-to-weight ratio [1] and the ability to cushion [2] and insulation [3]. This kind of structure is increasingly utilized as functional components in multiple industries [4]. Compared with traditional equal-material and subtractive manufacturing processes, 3D printing additive manufacturing exhibits significant flexibility for fabricating elaborate structures [5, 6]. Because of its low cost and ease of implementation, this technology has been widely used in the fabrication of porous structures [7].

Generally, porous structures can be divided into homogenious and heterogeneous according to the wall thickness [8]. Their difference is that the wall thickness of the homogenous porous structure is uniform, whereas that of the latter varies from each other. The homogeneous porous structure is the most widely utilized filling pattern because of its simplicity, which can be implemented by crosswise weaved paths in open-source software, such as Ultimaker Cura and Slic3r. Concerning the structural optimization, the regular geometry characteristic of homogenious porous structure limits the variable-density of materials. By contrast, the latter exhibits significant flexibility in optimizing the material layout. The typical theory to optimize the heterogeneous porous structure is the homogenization method [9]. The fundamental idea is to discretize the design domain into coarse meshes. Optimum wall thickness is calculated by translating topology optimization into a size optimization issue.

The complicated geometric characteristics decrease the printability of porous structures. Cross-section of porous structures is formed by thin walls. When the wall thickness is not an integer multiple of the path width, uneven filling occur [10, 11]. Additionally, the discontinuity of paths incurs virtual transition

lines and deposition defects at path start, which decreases the automation level and fiber integrity in continuous filament fabrication [12]. The porous structure consists of periodic grids formed by crossed paths. Consequently, a protuberance is incurred by material overlapping at intersections [13, 14]. The protuberance also hinders the subsequent nozzle movement and thus produces a shear force between the nozzle and the deposited material, even resulting in failure of the printing process [15].

A co-optimization method is developed to improve the structural stiffness and printability to manufacture graded-density porous structures. The fabrication process of 3D printing is considered by assigning wall thickness as a constant. The material layout is optimized by constructing graded Voronoi polygons according to the mechanical condition. Finally, a globally continuous path is proposed to fill porous structures.

2. Methodology

2.1. Manufacturing constraints

The manufacturing constraints of the filling path are cooperated according to the technical characteristics of 3D printing. To achieve path continuity and eliminate the uneven filling caused by the disparity of the printing area and path width, the wall thickness t of porous elements is specified as the double integer multiple of path width d.

2.2. Structural optimization

There is no regular form for Voronoi polygons. Since the Voronoi converge to a hexagon with the refinement of seed points [16], the hexagon is employed to approximately calculate the mechanical model of porous elements. The Gibson-Ashby model [17] is introduced to calculate the relationship between the elemental density and Young's modulus, which can be expressed by

$$\frac{E_{ij}^{w}}{E^{s}} = c\left(\frac{\rho_{ij}^{w}}{\rho_{ij}^{s}}\right)^{n} = c\left(\frac{t}{r_{ij}}\right)^{n} \tag{1}$$

where E stands for Young's modulus of porous elements; the empirical constants c and n are both tentatively taken as 1 in this study; ρ_{ij} denotes the filling density and area; w and s represent the porous element and solid element, respectively; r_{ij} replicate the distance between seed points.

Solid isotropic material with penalization algorithm (SIMP) [18] is introduced to calculate the relative optimum Young's modulus E_{ij}^{w}/E^{s}, which is expressed by the density x_{ij}.

Assuming that the smallest distance between seed points is r_{min}, then the x_{max} in SIMP is limited to

$$x_{max} = c\left(\frac{t}{r_{min}}\right)^{n} \tag{2}$$

r_{min} is taken as $2.5t$ in this study. The structural optimization is transformed to calculate the distance r_{ij} of seed points

$$r_{ij} = \frac{t}{c\left(x_{ij}\right)^{1/n}} \tag{3}$$

The graded Poisson-disk sampling method is introduced to generate variable-density seed points, aiming to construct the graded Voronoi elements according to x_{ij}.As shown in Figure 1(a), high-density seed points z_{ij} are uniformly placed in the design domain R^{o}, which is obtained by offsetting the original design domain R inwards the shell thickness h. Starting from an unvisited point z_{ij} with the smallest r_{ij}, z_{ij} is reserved in a new matrix, and other points inside the circle are removed. This step is repeated until removing all the seed points. Voronoi skeletons inside R^{o} are constructed by an open-source code *VoronoiLimit* [19], as shown in Figure 1(b).

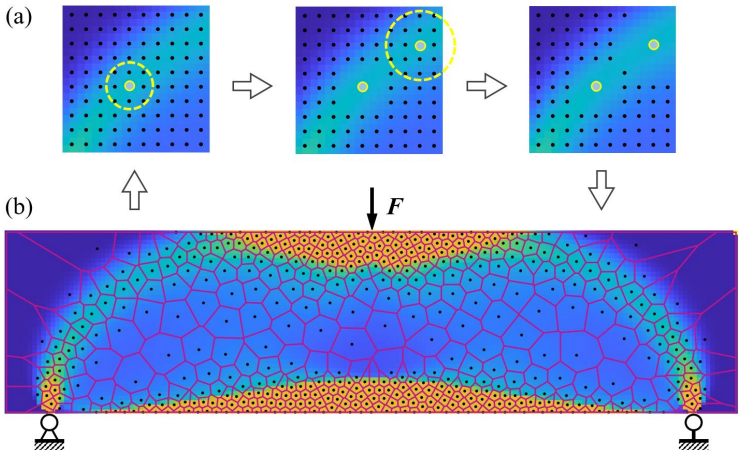

Figure 1: Graded Voronoi elements: (a) graded Poisson-disk sampling method; (b) result.

2.3. Filling ratio

Structural boundary and Voronoi polygons are offset inward $h - t/2$ and $t/2$ to generate the printing area. The filling ratio w_0 of porous structures relates to the density of seed points, which is determined by the relative Young's modulus x_{ij}. Therefore, x_{ij} in the SIMP algorithm needs to be recalculated to adjust the material layout. The dichotomy idea is introduced to adjust the $f^{(k)}$ of the SIMP

$$f^{(k)} = \frac{vol_1 + vol_2}{2} \quad \begin{cases} w_0^{(k)} < w_0, & vol_1 = f^{(k-1)} \\ w_0^{(k)} > w_0, & vol_2 = f^{(k-1)} \end{cases} \tag{4}$$

where (k) stands for the number of iterations; vol_1 and vol_2 express the minimum and maximum values of the interval, which are initially taken as 0 and x_{max}, respectively. The iteration ends when $\left|w_0^{(k)} - w_0\right| / w_0 \leq \varepsilon$. ε is a tolerance taken as 0.03.

2.4. Path optimization

The printing area and Voronoi polygons are offset inwards at an interval of d to generate discontinuous parallel paths. If the shortest distance between two adjacent paths is d, then the paths can be connected by adding a road, as shown in Figure 2. The connectable relationship of all the paths is counted in an adjacent matrix A, whose element is expressed by

$$a_{ij} = a_{ji} = \begin{cases} 1, & \text{paths are connectable} \\ 0, & \text{otherwise} \end{cases} \tag{5}$$

Starting from an arbitrary discontinuous path, other paths are connected to the current path one by one by introducing the depth-first search algorithm. To avoid the defects incurred by the road layer upon layer, their locations are randomly selected.

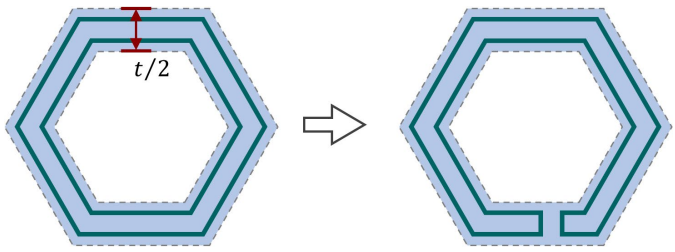

Figure 2: Path connection

3. Results and discussion

The MBB beam (160×40 mm) is employed to compare the path filling quality and mechanical performance of structures constructed by the co-optimization and the homegenization method[20]. The parameters are set as: w_0=0.35; d=0.4 mm; h=0.8 mm; t=0.8 mm. It should be noted that the comparison is conducted within a certain limit since the result is affected by parameters. The size of the periodic mesh in homegenization method is 5×5 mm, and the filling ratio of elements is limited to (0, 0.8]. The filling path is generated by an open-source software *Cura*, which consists of continuous contour parallel and gap-filling paths.

3.1. Path filling quality

Figure 3 shows the filling paths and printing results of various structures fabricated by polylactic acid with 10 mm thickness. Corresponding physical quantities of paths for one layer are listed in Table 1. Since the structure optimized by the homogenization method is composed of thin walls with changeable thickness, it is difficult to identify the connectable relationship. Consequently, the path is not globally continuous. And there are many intersections existing in the path. Furthermore, gap-filling paths incurred serious overfilling areas while decreasing underfilling areas, as reported in Table 1. By contrast, the co-optimization method offers a new way for solving these issues.

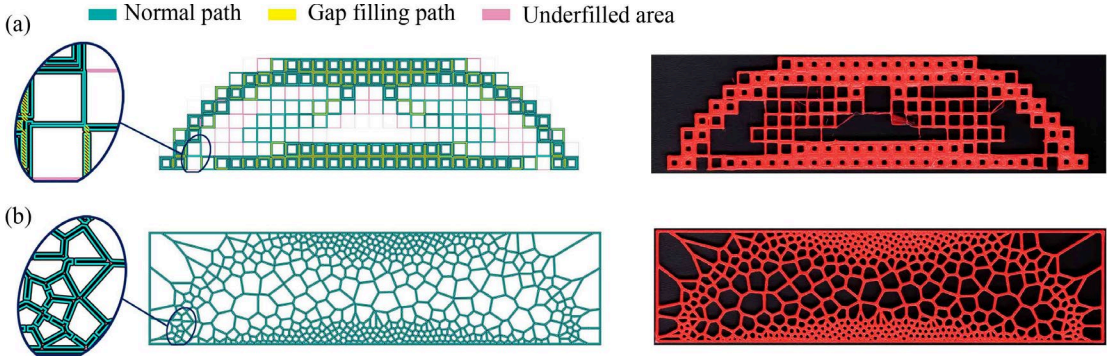

Figure 3: Filling paths and printing results: (a) homogenization method; (b) co-optimization method.

Table 1: Physical quantities of filling paths of various structures.

Factor	Path number	Intersection	Under-fill (%)	Over-fill (%)
homogenization	14	42	4.9	18.4
co-optimization	1	0	1.20	1.28

3.1. Mechanical performance

Finite element analysis (FEA) in-plane is employed to calculate the displacement of load points of various structures without considering the filling path. Smaller displacement indicates higher stiffness. It can be seen from Table 2 that their structural stiffnesses are similar. To further compare the mechanical performance, specimens shown in Figure 3 are tested by an electromechanical universal machine by applying a 1 mm/min displacement load, as shown in Figure 4. The structural stiffness is expressed by a mean slope when the displacement load is applied to 0.5, 1.0, and 1.5 mm. Deficiency of the critical mechanical component decreases the mechanical performance of structures optimized by the homogenization method. Consequently, structural stiffness and strength of porous structures constructed by the proposed method is better than that of its counterpart, as reported in Table 2

Table 2: Mechanical performance of various porous structures.

Factor	Load dispalcement	Stiffness (N/mm)	Strength (N)
homogenization	4.51	225	569
co-optimization	4.50	272	1052

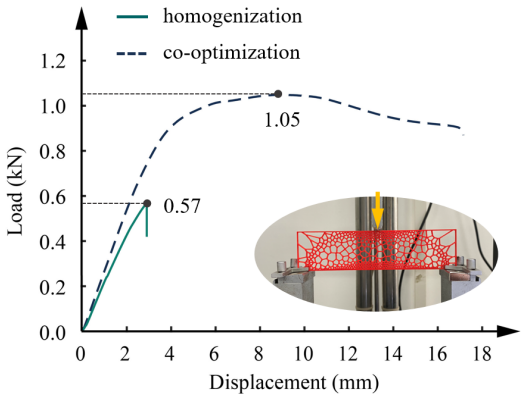

Figure 4: Mechanical test of various porous structures.

4. Conclusion

Material layout and printing quality significantly affect the mechanical performance of porous structures. A co-optimization method is proposed to design the porous strusture and ffilling path. The wall thickness of porous elements is specified as a constant according to the path width. The density of Voronoi elements is adaptively adjusted by the optimum Young's modulus under the manufacturing constraints. A customized filling path is developed to fabricate the optimized structure with high quality. The results indicate that the printing defects caused by the issue of the integer multiple of the path width, intersection, and discontinuity are adequately avoided. Specimens generated by the novel method exhibit the highest structural stiffness and strength due to the improvement in printing quality.

Acknowledgements

The paper is sponsored by the National Natural Science Foundation of China (grant number U20A20313).

References

[1] J. Zhang, Y. Shen, Y. Sun, et al. Design and mechanical testing of porous lattice structure with independent adjustment of pore size and porosity for bone implant[J]. Journal of Materials Research and Technology, 2022. 18: 3240-3255.

[2] H. Yin, W. Zhang, L. Zhu, et al. Review on lattice structures for energy absorption properties[J]. Composite Structures, 2023. 304: 116397.

[3] S. Rashidi, F. Hormozi, M. H. Doranehgard. Abilities of porous materials for energy saving in advanced thermal systems[J]. Journal of thermal analysis and calorimetry, 2021. 143: 2437-2452.

[4] D. Chen, K. Gao, J. Yang, et al. Functionally graded porous structures: analyses, performances, and applications–a review[J]. Thin-Walled Structures, 2023. 191: 111046.

[5] I. Gibson, D. Rosen, B. Stucker, et al. Design for additive manufacturing[J]. Additive manufacturing technologies, 2021: 555-607.

[6] G. Liu, X. Zhang, X. Chen, et al. Additive manufacturing of structural materials[J]. Materials Science and Engineering: R: Reports, 2021. 145: 100596.

[7] R. Guerra Silva, M. J. Torres, J. Zahr Viñuela, et al. Manufacturing and characterization of 3D miniature polymer lattice structures using fused filament fabrication[J]. Polymers, 2021. 13(4): 635.

[8] Y. Tang, S. Yang, Y. F. Zhao. Design method for conformal lattice-skin structure fabricated by AM technologies[C]. International Design Engineering Technical Conferences and Computers and Information in Engineering Conference. American Society of Mechanical Engineers. 2016: V01AT02A037.

[9] P. Zhang, J. Toman, Y. Yu, et al. Efficient design-optimization of variable-density hexagonal cellular structure by additive manufacturing: theory and validation[J]. Journal of Manufacturing Science and Engineering, 2015. 137(2): 021004.

[10] J. V. Carstensen. Topology optimization with nozzle size restrictions for material extrusion-type additive manufacturing[J]. Structural and Multidisciplinary Optimization, 2020. 62(5): 2481-2497.

[11] E. Fernández, C. Ayas, M. Langelaar, et al. Topology optimisation for large-scale additive manufacturing: generating designs tailored to the deposition nozzle size[J]. Virtual and Physical Prototyping, 2021. 16(2): 196-220.

[12] N. Li, G. Link, T. Wang, et al. Path-designed 3D printing for topological optimized continuous carbon fibre reinforced composite structures[J]. Composites Part B: Engineering, 2020. 182: 107612.

[13] R. Li, G. Wang, Y. Ding, et al. Optimization of the geometry for the end lateral extension path strategy to fabricate intersections using laser and cold metal transfer hybrid additive manufacturing[J]. Additive Manufacturing, 2020. 36: 101546.

[14] G.-H. Song, C.-M. Lee, D.-H. Kim. Investigation of path planning to reduce height errors of intersection parts in wire-Arc Additive manufacturing[J]. Materials, 2021. 14(21): 6477.

[15] Y. Wang, G. Zhang, H. Ren, et al. Fabrication strategy for joints in 3D printed continuous fiber reinforced composite lattice structures[J]. Composites Communications, 2022. 30: 101080.

[16] A. M. Bronstein, M. M. Bronstein, R. Kimmel. Numerical geometry of non-rigid shapes[M]. First edition. New York: Springer Science & Business Media, 2008: 46-51.

[17] L. J. Gibson, M. F. Ashby. Cellular solids: structure and properties [M]. Second Edition. Cambridge University Press.

[18] E. Andreassen, A. Clausen, M. Schevenels, et al. Efficient topology optimization in MATLAB using 88 lines of code[J]. Structural and Multidisciplinary Optimization, 2011. 43: 1-16.

[19] J. Sievers. VoronoiLimit (varargin)[CP]. (2020-06-08). MATLAB Central File Exchange. https://www.mathworks.com/matlabcentral/fileexchange/34428-voronoilimit-varargin. (Accessed date: 2023-12-26). .].

[20] G. Dong, Y. Tang, Y. F. Zhao. A 149 line homogenization code for three-dimensional cellular materials written in MATLAB[J]. Journal of Engineering Materials and Technology, 2019. 141(1): 011005.